BOUNDARY-VALUE PROBLEMS

Many problems in electrical engineering require solution of integral or differential equations which describe physical phenomena. The choice whether integral or differential equations are used to formulate and solve specific problems depends on many factors, whose discussion is beyond the scope of this article. This article strictly concentrates on the use of the finite-difference method (FDM) in the numerical analysis of boundary-value problems associated with primarily static and to some extent quasistatic electromagnetic (EM) fields. Although all examples presented herein deal with EM-related engineering applications, some numerical aspects of FDM are also covered. Since there is a wealth of literature in numerical and applied mathematics about the FDM, little will be said about the theoretical aspects of finite differencing. Such issues as the proof of existence or convergence of the numerical solution will not be covered, while the appropriate references will be provided to the interested reader. Instead, the coverage of FDM will deal with the details about implementation of numerical algorithms, compact storage schemes for large sparse matrices, the use of open boundary truncation, and efficient handling of inhomogeneous and anisotropic materials.

The emphasis will be placed on the applications of FDM to three-dimensional boundary-value problems involving objects with arbitrary geometrical shapes that are composed of complex dielectric materials. Examples of such problems include modeling of discrete passive electronic components, semiconductor devices and their packages, and cross-talk in multiconductor transmission lines. When the wavelength of operation is larger than the largest geometrical dimensions of the object that is to be modeled, static or quasistatic formulation of the problem is appropriate. In electrostatics, for example, this implies that the differential equation governing the physics (voltage distribution) is of Laplace type for the source-free environment and of Poisson type in regions containing sources. The solution of such second-order partial differential equations can be readily obtained using the FDM.

Although the application of FDM to homogeneous materials is simple, complexities arise as soon as inhomogeneity and anisotropy are introduced. The following discussion will provide essential details on how to overcome any potential difficulties in adapting FDM to boundary-value problems involving such materials. The analytical presentation will be supplemented with abundant illustrations that demonstrate how to implement the theory in practice. Several examples will also be provided to show the complexity of problems that can be solved by using FDM.

BRIEF HISTORY OF FINITE DIFFERENCING IN ELECTROMAGNETICS

The utility of the numerical solution to partial differential equations (or PDEs) utilizing finite difference approximation to partial derivatives was recognized early (1). Improvements to the initial iterative solution methods, discussed in Ref. 1, by using relaxation were subsequently introduced (2,3). However, before digital computers became available, the applications of the FDM to the solution of practical boundary-value problems was a tedious and often impractical task. This was especially true if high level of accuracy were required.

With the advent of digital computers, numerical solution of PDEs became practical. They were soon applied to various problems in electrostatics and quasistatics such as in the analysis of microstrip transmission lines (4), among many others. The FDM found quick acceptance in the solution of boundary-value problems within regions of finite extent, and efforts were initiated to extend their applicability to open region problems as well (5).

As a point of departure, it is interesting to note that some of the earliest attempts to obtain the solution to practical boundary-value problems in electrostatics involved experimental methods. They included the electrolytic tank approach and resistance network analog technique (6), among others, to simulate the finite difference approximations to PDEs.

Finally, it should be mentioned that in addition to the application of FDM to static and quasistatic problems, the FDM was also adapted for use in the solution of dynamic, full-wave EM problems in time and frequency domain. Most notably, the use of finite differencing was proposed for the solution to Maxwell's curl equations in the time domain (7). Since then, a tremendous amount of work on the finite-difference time-domain (or FD-TD) approach was carried out in diverse areas of electromagnetics. This includes antennas and radiation, scattering, microwave integrated circuits, and optics. The interested reader can consult the authoritative work in Ref. 8, as well as other articles on eigenvalue and related problems in this encyclopedia, for further details and additional references.

ENGINEERING BASICS OF FINITE DIFFERENCING

It is best to introduce the FDM for the solution of engineering problems, which deal with static and quasistatic electromagnetic fields, by way of example. Today, just about every ele-

mentary text in electromagnetics—as well as newer, more numerically focused introductory EM textbooks—will have a discussion on FDM (e.g., pp. 241–246 of Ref. 9 and Section 4.4 of Ref. 10) and its use in electrostatics, magnetostatics, waveguides, and resonant cavities. Regardless, it will be beneficial to briefly go over the basics of electrostatics for the sake of completeness and to provide a starting point for generalizing FDM for practical use.

GOVERNING EQUATIONS OF ELECTROSTATICS

The analysis of electromagnetic phenomena has its roots in the experimental observations made by Michael Faraday. These observations were cast into mathematical form by James Clerk Maxwell in 1873 and verified experimentally by Heinrich Hertz 25 years later. When reduced to electrostatics, they state that the electric field at every point in space within a homogeneous medium obeys the following differential equations (9):

$$\nabla \times \vec{E} = 0 \tag{1}$$

$$\nabla \cdot \epsilon_0 \epsilon_r \vec{E} = \rho_v \tag{2}$$

where ρ_v is the volumetric charge density, ϵ_0 ($\approx 8.854 \cdot 10^{-12}$ Farads/m) is the permittivity of freespace, and ϵ_r is the relative dielectric constant. The use of the vector identity $\nabla \times \nabla\phi \equiv 0$ in Eq. (1) allows for the electric field intensity, $\vec{E}$ (volts/m), to be expressed in terms of the scalar potential $\vec{E} = -\nabla\phi$. When this is substituted for the electric field in Eq. (2), a second-order PDE for the potential ϕ is obtained:

$$\nabla \cdot (\epsilon_r \nabla\phi) = -\rho_v/\epsilon_0 \tag{3}$$

which is known as the Poisson equation. If the region of space, where the solution for the potential is sought, is source-free and the dielectric is homogeneous (i.e., ϵ_r is constant everywhere), Eq. (3) reduces to the Laplace equation $\nabla^2\phi = 0$.

The solution to the Laplace equation can be obtained in several ways. Depending on the geometry of the problem, the solution can be found analytically or numerically using integral or differential equations. In either case, the goal is to determine the electric field in space due to the presence of charged conductors, given that the voltage on their surface is known. For example, if the boundaries of the charged conductors are simple shapes, such as a rectangular box, circular cylinder, or a sphere, then the boundary conditions (constant voltage on the surface) can be easily enforced and the solution can be obtained analytically. On the other hand, when the charged object has an irregular shape, the Laplace equation cannot be solved analytically and numerical methods must be used instead.

The choice as to whether integral or differential equation formulation is used to determine the potential heavily depends on the geometry of the boundary-value problem. For example, if the charged object is embedded within homogeneous medium of infinite extent, integral equations are the preferable choice. They embody the boundary conditions on the potential ϕ at infinity and reduce the numerical effort to finding the charge density on the surface of the conductor (see Sections 5.2 or 4.3 of Ref. 9 or 10 for further details).

On the other hand, when the boundary-value problem includes inhomogeneous dielectrics (i.e., ϵ_r varying from point to point in space), the surface integral equation methods are no longer applicable (or are impractical). Instead, such problems can be formulated using volumetric PDE solvers such as the FDM.

It is important to note that similar considerations (to those stated above) also apply to the solution of the Poisson equation. In this case, in addition to the integration over the conductor boundaries, integration over the actual sources (charge density) must also be performed. The presence of the sources has the same effects on PDEs and FDM, as their effects must be taken into account at all points in space where they exist.

Direct Discretization of Governing Equation

To illustrate the utility and limitations of FDM and to introduce two different ways of deriving the numerical algorithm, consider the geometry shown in Fig. 1. Note that for the sake of clarity and simplicity, the initial discussion will be restricted to two dimensions.

The infinitely long, perfectly conducting circular cylinder in Fig. 1 is embedded between two dielectrics. To determine the potential everywhere in space, given that the voltage on the cylinder surface is V_0, the FDM will be used. There are two approaches that might be taken to develop the FDM algorithm. One approach would be to solve Laplace (or Poisson) equations in each region of uniform dielectric and enforce the boundary conditions at the interface between them. The other route would involve development of a general volumetric algorithm, which would be valid at every point in space, including the interface between the dielectrics. This would involve seeking the solution of a single, Laplace-type (or Poisson) differential equation:

$$\nabla \cdot (\epsilon_r(x,y)\nabla\phi) = \epsilon_r(x,y)\left(\frac{\partial^2\phi}{\partial x^2} + \frac{\partial^2\phi}{\partial y^2}\right) + \left(\frac{\partial\epsilon_r}{\partial x}\frac{\partial\phi}{\partial x} + \frac{\partial\epsilon_r}{\partial y}\frac{\partial\phi}{\partial y}\right) = \begin{cases} 0 \\ -\dfrac{\rho(x,y)}{\epsilon_0} \end{cases} \tag{4}$$

which is valid everywhere, except for the surface of the conductor.

The numerical approach to solving Eq. (4) starts with the approximation to partial derivatives using finite differences.

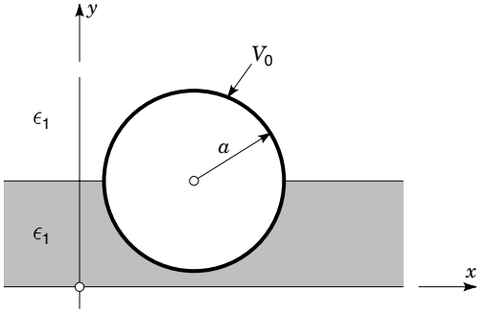

Figure 1. Charged circular cylinder embedded between two different dielectrics.

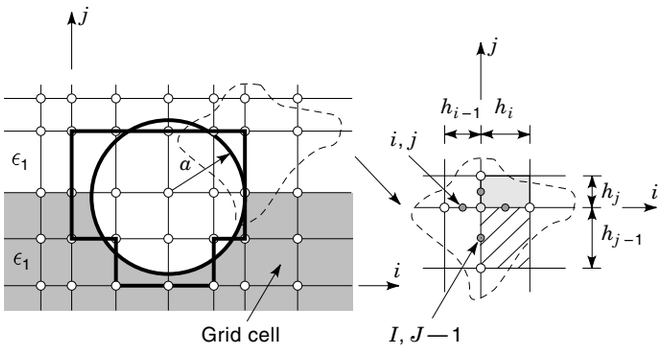

Figure 2. "Staircase" approximation to boundary of circular cylinder and notation for grid dimensions.

This requires some form of discretization for the space (area or volume in two or three dimensions) where the potential is to be computed. The numerical solution of the PDE will lead to the values of the potential at a finite number of points within the discretized space. Figure 2 shows one possible discretization scheme for the cylinder in Fig. 1 and its surroundings. The points form a two-dimensional (2-D) grid and they need not be uniformly spaced. Note that the grid points, where the potential is to be computed, have to be defined all along the grid lines to allow for properly approximating the derivatives in Eq. (4). In other words, the grid lines cannot abruptly terminate or become discontinuous within the grid.

Using finite differences, the first-order derivative at any point in the grid can be approximated as follows:

$$\left(\frac{\partial\phi}{\partial x}\right)_{i,j} \approx \frac{(\phi_{I_1,J} - \phi_{I-1,J})}{(h_i + h_{i-1})/2} = \left[\left(\frac{\phi_{i+1,j} + \phi_{i,j}}{2}\right) - \left(\frac{\phi_{i,j} + \phi_{i-1,j}}{2}\right)\right] \frac{1}{(h_i + h_{i-1})/2} = \frac{\phi_{i+1,j} - \phi_{i-1,j}}{h_i + h_{i-1}} \tag{5}$$

with the help of intermediate points I, J (black circles in Fig. 2). The approximation for the second derivatives can be obtained in a similar manner and is given by

$$\left[\frac{\partial}{\partial x}\left(\frac{\partial\phi}{\partial x}\right)\right]_{i,j} \approx \frac{\left(\frac{\partial\phi}{\partial x}\right)_{I+1,J} - \left(\frac{\partial\phi}{\partial x}\right)_{I-1,J}}{(h_i + h_{i-1})/2} = \left[\left(\frac{\phi_{i+1,j} - \phi_{i,j}}{h_i}\right) - \left(\frac{\phi_{i,j} - \phi_{i-1,j}}{h_{i-1}}\right)\right] \times \frac{1}{(h_i + h_{i-1})/2} \tag{6}$$

Once all derivatives in Eq. (4) are replaced with their respective finite-difference approximations and all similar terms are grouped together, the discrete version of Eq. (4) takes on the following form:

$$\phi_{i,j} \approx \frac{1}{Y_{i,j}}(Y_{i+1}\phi_{i+1,j} + Y_{i-1}\phi_{i-1,j} + Y_{j+1}\phi_{i,j+1} + Y_{j-1}\phi_{i,j-1}) + \begin{cases} 0 \\ \dfrac{(\rho_{i,j} + \rho_{i-1,j} + \rho_{i,j-1} + \rho_{i-1,j-1})}{\epsilon_0} \end{cases} \tag{7}$$

In the above equation, the Y factors contain the material parameters and distances between various adjacent grid points. They are expressed below in a compact form:

$$Y_{i\pm1} = \frac{2}{(h_i + h_{i-1})^2}\left\{(\epsilon_{i,j-1} + \epsilon_{i,j})\begin{pmatrix}\dfrac{3h_i + h_{i-1}}{h_i} \\ \dfrac{h_i - h_{i-1}}{h_{i-1}}\end{pmatrix} + (\epsilon_{i-1,j-1} + \epsilon_{i-1,j})\begin{pmatrix}\dfrac{h_{i-1} - h_i}{h_i} \\ \dfrac{h_i + 3h_{i-1}}{h_{i-1}}\end{pmatrix}\right\} \tag{8}$$

$$Y_{j\pm1} = \frac{2}{(h_j + h_{j-1})^2}\left\{(\epsilon_{i-1,j} + \epsilon_{i,j})\begin{pmatrix}\dfrac{3h_j + h_{j-1}}{h_j} \\ \dfrac{h_j - h_{j-1}}{h_{j-1}}\end{pmatrix} + (\epsilon_{i-1,j-1} + \epsilon_{i,j-1})\begin{pmatrix}\dfrac{h_{j-1} - h_j}{h_j} \\ \dfrac{h_j + 3h_{j-1}}{h_{j-1}}\end{pmatrix}\right\} \tag{9}$$

$$Y_{i,j} = Y_{i+1,j} + Y_{i-1,j} + Y_{i,j+1} + Y_{i,j-1} \tag{10}$$

It is important to add that in deriving the above equations, a particular convention for associating the medium parameters to individual grid cells was employed. Specifically, it was assumed that the medium parameter values of the entire grid cell were associated with (or assigned to) the lower left corner of that cell. For example, $\epsilon_{i,j}$ is assumed to be constant over the shaded grid cell area shown in Fig. 2, while $\epsilon_{i,j-1}$ is constant over the hatched area, which is directly below.

Observe what are the consequences of converting the continuous PDE given in Eq. (4) to its approximate discrete form stated in Eq. (7). First, the boundary-value problem over the continuous space, shown in Fig. 1, was "mapped" onto a discrete grid (see Fig. 2). Clearly, if the number of grid points increases, then spacing between them will become smaller. This provides a better approximation to the actual continuous problem. In fact, in the limit as the number of grid point reaches infinity, the discrete and continuous problems become identical.

In addition to illustrating the "mapping" of a continuous problem to its discrete analog, Fig. 2 also clearly demonstrates one of FDM's undesirable artifacts. Note that objects with smooth surfaces are replaced with a "staircased" approximation. Obviously, this approximation can be improved by reducing the discretization grid spacing. However, this will increase the number of points where the potential has to be calculated, thus increasing the computational complexity of the problem. One way to overcome this is to use a nonuniform discretization, as depicted in Fig. 2. Specifically, finer discretization can be used in the region near the smooth surface of the cylinder to better approximate its shape, followed by gradually increasing the grid point spacing between the cylinder and grid truncation boundary.

At this point, it is also appropriate to add that other, more rigorous methods have been proposed for incorporating curved surfaces into the finite-difference type of algorithms. They are based on special-purpose differencing schemes,

which are derived by recasting the same PDEs into their equivalent integral forms. They exploit the surface or contour integration and are used to replace the regular differencing algorithm on the curved surfaces or contours of smooth objects. This approach was already implemented for the solution of dynamic full-wave problems (11) and could be adapted to electrostatic boundary-value problems as well.

Finally, Eq. (7) also shows that the potential at any point in space, which is source-free, is a weighted average of the potentials at the neighboring points only. This is typical of PDEs, because they only represent physical phenomena locally—that is, in the immediate vicinity of the point of interest. As will be shown later, one way to "propagate" the local information through the grid is to use an iterative scheme. In this scheme, the known potential, such as V_0 at the surface of the conducting cylinder in Fig. 1, is carried throughout the discretized space by stepping through all the points in the grid. The iterations are continued until the change in the potential within the grid is very small.

"Indirect" Discretization of Governing Equation

As shown in the previous section, appropriate finite-difference approximations were required for the first- and second-order derivatives in order to convert Eq. (4) to a discrete form. Intermediate points (I, J) were used midway between the regular grid nodes for obtaining average values of the potential, its first derivatives, and dielectric constants to facilitate the derivation of the final update equation for the potential. This can be avoided and an alternative, but equally valid finite differencing scheme to that given in Eq. (7), which for the sake of brevity is restricted to the Laplace equation only, can be obtained. The first step is to simplify Eq. (4) by recasting it into an integrodifferential form. To achieve this, Eq. (4) should be integrated over a volume, which completely encloses any one of the grid nodes. This will be referred to as the volume of the unit cell (V_U), which is bounded by surface S_U (see Fig. 3). Stoke's theorem is applied to replace the volume integration by a surface integral:

$$\begin{aligned}\int_{V_U} \nabla \cdot (\epsilon_r(x,y)\nabla\phi)\, dv &= \oint_{S_U} (\epsilon_r(x,y)\nabla\phi) \cdot \hat{n}\, ds \\ &= \oint_{S_U} \epsilon_r(x,y)\frac{\partial\phi}{\partial n} ds = 0\end{aligned} \tag{11}$$

where $\hat{n}$ is the unit vector, normal to S_U and pointing out of it.

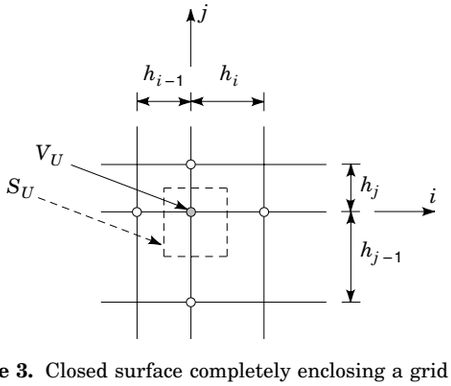

Figure 3. Closed surface completely enclosing a grid node.

To illustrate this "indirect" discretization procedure in 2-D, consider surface $S_{Ui,j}$ (that is, just a contour) shown in Fig. 3, which completely encloses grid point i, j. The integral in Eq. (11) reduces to four terms, each corresponding to one of the faces of $S_{Ui,j}$. For example, the integral over the right edge (or face) of $S_{Ui,j}$ can be approximated as

$$\frac{\phi_{i+1,j} - \phi_{i,j}}{h_i}\left(\frac{h_{j-1}}{2}\epsilon_{i,j-1} + \frac{h_j}{2}\epsilon_{i,j}\right) \tag{12}$$

When the remaining integrals are evaluated and the like terms are grouped together, the final form of the "indirect" FDM algorithm is obtained. This algorithm is identical in form to that given earlier in Eq. (7). However, the weighting Y factors are different from those appearing in Eqs. (8) and (9). Their complete expressions are given by

$$Y_{\left\{\begin{smallmatrix} i+1 \\ i-1 \end{smallmatrix}\right\}} = \left(h_{j-1}\epsilon_{\left\{\begin{smallmatrix} i,j-1 \\ i-1,j-1 \end{smallmatrix}\right\}} + h_j\epsilon_{\left\{\begin{smallmatrix} i,j \\ i-1,j \end{smallmatrix}\right\}}\right)\frac{1}{2h_{\left\{\begin{smallmatrix} i \\ i-1 \end{smallmatrix}\right\}}} \tag{13}$$

with $Y_{i,j}$ being the sum of all other Y's, the same as before [see Eq. (10)].

It should be added that this approach has been suggested several times in the literature—for example, in Refs. 12 and 13. Therein, Eq. (11) was specifically used to enforce the boundary conditions at the interface between different dielectrics only in order to "connect" FDM algorithms based on the Laplace equation for the homogeneous regions. However, there is no reason not to use Eq. (11) at every point in space, especially if the boundary-value problem involves inhomogeneous media. This form of FDM scheme is completely analogous to that presented in the previous section. In fact, it is a little simpler to derive and involves a fewer number of arithmetic operations.

Numerical Implementation in Two-Dimensions

There are several important numerical issues that must be addressed prior to implementing FDM on the computer. Such questions as how to terminate the grid away from the region of interest and which form of the FDM algorithm to choose must be answered first. The following discussion provides some simple answers, postponing the more detailed treatment until later.

Simplistic Grid Boundary Truncation. Clearly, since even today's computers do not have infinite resources, the computational volume (or space) must somehow be terminated (see Fig. 4). The simplest approach is to place the truncation boundary far away from the region of interest and to set the potential on it equal to zero. This approach is valid as long as the truncation boundary is placed far enough not to interact with the charged objects within, as for example the "staircased" cylinder shown in Fig. 4. The downside of this approach is that it leads to large computational volumes, thereby requiring unnecessarily high computer resources. This problem can be partly overcome by using a nonuniform grid, with progressively increasing spacing from the cylinder toward the truncation boundary. It should be added that there are other ways to simulate the open-boundary conditions, which is an advanced topic and will be discussed later.

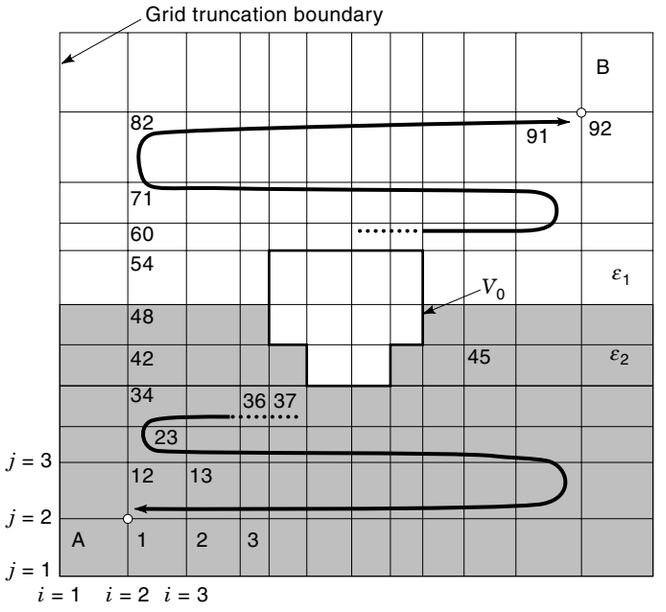

Figure 4. Complete discretized geometry and computational space for cylinder in Fig. 2.

Iteration-Based Algorithm. Several iteration methods can be applied to solve Eq. (7), each leading to different convergence rates (i.e., how fast an acceptable solution is obtained). A complete discussion of this topic, as well as of the accuracy of the numerical approximations in FDM, appears in Ref. 14 and will not be repeated here. The interested reader may also find Ref. 15 quite useful, because it covers such topics in more rigorous detail and includes a comprehensive discussion on the proof of the existence of the finite-differencing solution to PDEs. However, for the sake of brevity, this article deals with the most popular and widely used approach, which is called successive overrelaxation (SOR) (see, e.g., Ref. 14).

SOR is based on Eq. (7), which is rearranged as

$$\begin{aligned}\phi_{i,j}^{p+1} &\approx \phi_{i,j}^{p} + \frac{\Omega}{Y_{i,j}}(Y_{i+1}\phi_{i+1,j}^{p} + Y_{i-1}\phi_{i-1,j}^{p+1} + Y_{j+1}\phi_{i,j+1}^{p} \\ &\quad + Y_{j-1}\phi_{i,j-1}^{p+1} - Y_{i,j}\phi_{i,j}^{p}) \\ &= (1-\Omega)\phi_{i,j}^{p} + \frac{\Omega}{Y_{i,j}}(Y_{i+1}\phi_{i+1,j}^{p} + Y_{i-1}\phi_{i-1,j}^{p+1} \\ &\quad + Y_{j+1}\phi_{i,j+1}^{p} + Y_{j-1}\phi_{i,j-1}^{p+1})\end{aligned} \tag{14}$$

In the above equation, superscripts p and $p+1$ denote the present and previous iteration steps and Ω is the so-called overrelaxation factor, whose value can vary from 1 to 2. Note that Ω accelerates the change in the potential from one iteration to the next at any point in the grid. It can be a constant throughout the entire relaxation (solution) process or be varying according to some heuristic scheme. For example, it was found that the overall rate of convergence is improved by setting Ω near 1.8 at the start of the iteration process and gradually reducing it to 1.2 with the numbers of iterations.

At this point, the only remaining task is to define the appropriate criteria for terminating the FDM algorithm. Although there are rigorous ways of selecting the termination criterion, the following approach, which seems to work quite well, is presented instead. As stated below, it is based on calculating the change in the potential between successive iterations at every point in the grid and comparing the maximum value to the (user-selectable) error criterion:

$$\mathrm{ERR}_{\max} = \sum_{i=1}^{N_x}\sum_{j=1}^{N_y}\max(|\phi_{i,j}^{p+1} - \phi_{i,j}^{p}|) \tag{15}$$

Regardless of it being simple, the redeeming feature of this approach is that the error is computed globally within the grid, rather than within a particular single grid node. The danger in monitoring the convergence of the algorithm at a single node may lead to premature termination or to an unnecessarily prolonged execution.

Now that an error on which the algorithm termination criterion is based has been defined, the iteration process can be initiated. Note that there are several ways to "march" through the grid. Specifically, the updating of the potential may be started from point A, as shown in Fig. 4, and end at point B, or vice versa. If the algorithm works in this manner, the solution will tend to be artifically "biased" toward one region of the grid, with the potential being "more converged" in regions where the iteration starts. The obvious way to avoid this is to change the direction of the "marching" process after every few iterations. As a result, the potential will be updated throughout the grid uniformly and will converge at the same rate. Note from Fig. 4 that the potential only needs to be computed at the internal points of the grid, since the potential at the outer boundary is (for now) assumed to be zero. Moreover, it should also be evident that the potential at the surface of the cylinder, as well as inside it, is known (V_0) and need not be updated during the iteration process.

Matrix-Based Algorithm. Implementation of the finite-difference algorithms is not restricted to relaxation techniques only. The solution of Eq. (4) for the electrostatic potential can also be obtained using matrix methods. To illustrate this, the FDM approximation to Eq. (4)—namely, Eq. (7)—will be rewritten as

$$\begin{aligned}(Y_{i+1}\phi_{i+1,j} + Y_{i-1}\phi_{i-1,j} + Y_{j+1}\phi_{i,j+1} + Y_{j-1}\phi_{i,j-1}) \\ - Y_{i,j}\phi_{i,j} \approx 0\end{aligned} \tag{16}$$

The above equation must be enforced at every internal point in the grid, except at the surface of and internal to the conductors, where the potential is known (V_0). For the particular example of the cylinder shown in Fig. 4, these points are numbered 1 through 92. This implies that there are 92 unknowns, which must be determined. To accomplish this, Eq. (16) must be enforced at 92 locations in the grid, leading to a system of 92 linear equations that must be solved simultaneously.

To demonstrate how the equations are set up, consider nodes 1, 36, and 37 in detail. At node 1 (where $i = j = 2$), Eq. (16) reduces to

$$Y_3^i\phi_{12} + Y_3^j\phi_2 - Y_{2,2}\phi_1 = 0 \tag{17}$$

where the fact that the potential at the outer boundary nodes $(i, j) = (1, 2)$ and $(2, 1)$ is zero was taken into account and superscripts i and j on Y's were introduced as a reminder

whether they correspond to $Y_{i\pm1}$ or $Y_{j\pm1}$. In addition, the potential at nodes $(i, j) = (2, 2)$, $(3, 2)$ and $(2, 3)$ was also relabeled as ϕ_1, ϕ_2, and ϕ_{12}, respectively. Similarly, at nodes 36 $(i, j = 4, 5)$ and 37 $(i, j = 5, 5)$, Eq. (16) becomes

$$Y_5^i\phi_{37} + Y_3^i\phi_{35} + Y_6^j\phi_{44} + Y_4^j\phi_{25} - Y_{4,5}\phi_{36} = 0 \tag{18}$$

and

$$Y_4^i\phi_{36} + Y_4^j\phi_{26} - Y_{5,5}\phi_{37} = -Y_6^iV_0 - Y_6^jV_0 = V_{37} \tag{19}$$

where in Eq. (19) the known quantities (the potentials on the surface of the cylinder at nodes 5, 6 and 6, 5) were moved to the right-hand side.

Similar equations can be obtained at the remaining free grid nodes where the potential is to be determined. Once Eq. (16) has been enforced everywhere within the grid, the resulting set of equations can be combined into the following matrix form:

$$\begin{bmatrix} -Y_{2,2} & Y_3^j & 0 & \cdot & 0 & Y_3^i & 0 & \cdot & & & & & & & & & & & & & & & \cdot & 0 \\ & & & & & & & & & & & & & & & & & & & & & & & \\ 0 & 0 & \cdot & \cdot & 0 & 0 & 0 & Y_4^j & 0 & \cdot & 0 & Y_3^i & -Y_{4,5} & Y_5^i & 0 & \cdot & 0 & Y_6^j & 0 & \cdot & \cdot & 0 \\ 0 & 0 & \cdot & \cdot & 0 & 0 & 0 & 0 & Y_4^j & 0 & \cdot & 0 & Y_4^i & -Y_{5,5} & 0 & \cdot & \cdot & 0 & \cdot & \cdot & \cdot & 0 \\ & & & & & & & & & & & & & & & & & & & & & & & \end{bmatrix} \begin{bmatrix} \phi_1 \\ \phi_2 \\ \cdot \\ \cdot \\ \cdot \\ \phi_{12} \\ \cdot \\ \phi_{25} \\ \phi_{26} \\ \cdot \\ \cdot \\ \phi_{35} \\ \phi_{36} \\ \phi_{37} \\ \cdot \\ \cdot \\ \cdot \\ \phi_{44} \\ \cdot \\ \phi_{92} \end{bmatrix} = \begin{bmatrix} 0 \\ \cdot \\ \\ \\ \\ \\ \\ \\ \\ \\ \\ \cdot \\ 0 \\ V_{37} \\ \cdot \\ \\ \\ \\ \\ 0 \end{bmatrix} \tag{20}$$

which can be written more compactly as

$$[Y][\phi] = [V_0] \tag{21}$$

Clearly, the coefficient matrix of the above system of equations is very sparse, containing few nonzero elements. In fact, for boundary-value problems in two dimensions with isotropic dielectrics, there will be at most five nonzero terms in a single row of the matrix. Although standard direct matrix solution methods, such as Gauss inversion of LU decomposition and back-substitution, can be applied to obtain the solution to Eq. (20), they are wasteful of computer resources. In addition to performing many unnecessary numerical operations with zeroes during the solution process, a large amount of memory has to be allocated for storing the coefficient matrix. This can be avoided by exploiting the sparsity of the coefficient matrix, using well-known sparse matrix storage techniques, and taking advantage of specialized sparse matrix algorithms for direct (16) or iterative (17–19) solution methods.

Since general-purpose solution techniques for sparse linear equation systems are well-documented, such as in Refs. 16–19, they will not be discussed here. Instead, the discussion will focus on implementation issues specific to FDM. In particular, issues related to the efficient construction of the $[Y]$ matrix in Eq. (20) and to the sparsity coding scheme are emphasized.

In the process of assembling $[Y]$, as well as in the postprocessing computations such as in calculating the E field, it is necessary to quickly identify the appropriate entries ϕ_k within the vector $[\phi]$, given their locations in the grid (i, j). Such searching operations are repeated many times, as each element of $[Y]$ is stored in its appropriate location. Note that the construction of $[Y]$, in large systems (500–5000 equations), may take as much CPU time as the solution itself. Thus, optimization of the search for index locations is important.

One approach to quickly find a specific number in an array of N numbers is based on the well-known Bisection Search Algorithm (Section 3.4 in Ref. 17). This algorithm assumes that the numbers in the array are arranged in an ascending order and requires, at most, $\log_2(N)$ comparisons to locate a particular number in the array. In order to apply this method, a mapping that assigns a unique code to each allowable combination of the grid coordinates i, j is defined. One such mapping is

$$\text{code} = i \cdot N_y + j \tag{22}$$

where N_y is the total number of grid points along the j direction. The implementation of this algorithm starts by defining two integer arrays: CODE and INDEX. The array CODE holds the identification codes [computed from Eq. (22)], while INDEX contains the corresponding value of k. Both CODE and INDEX are sorted together so that the elements of CODE are rearranged to be in an ascending order. Once generated and properly sorted, these arrays can be used to find the index k (to identify ϕ_k) for grid coordinates (i, j) in the following manner:

1. Given i and j, compute *code* $= i \cdot N_y + j$.
2. Find the array index m, such that *code* $=$ CODE(m), using the Bisection Search Algorithm.

3. Look up k using $k = \text{INDEX}(m)$, thereby identifying the appropriate ϕ_k, given i, j.

The criteria for selecting a particular sparsity coding scheme for the matrix [Y] are (a) the minimization of storage requirements and (b) optimization of matrix operations—in particular, multiplication and LU factoring. One very efficient scheme is based on storing [Y] using four one-dimensional arrays:

1. Real array DIAG(i) = diagonal entry of row i
2. Real array OFFD(i) = ith nonzero off-diagonal entry (scanned by rows)
3. Integer array IROW(i) = index of first nonzero off-diagonal entry of row i
4. Integer array ICOL(i) = column number of ith nonzero off-diagonal entry (scanned by rows)

Assuming a system of N equations, the arrays DIAG, IROW, OFFD, and ICOL have N, $N + 1$, $4N$, and $4N$ entries, respectively. Therefore, the total memory required to store a sparsity coded matrix [Y] is approximately $40N$ bytes (assuming 32-bit storage for both real and integer numbers). On the other hand, $4N^2$ bytes would be needed to store the full form of [Y]. For example, in a system with 1000 equations, the full storage mode requires 4 megabytes, while the sparsity coded matrix occupies only 40 kilobytes of computer memory.

Perhaps the most important feature of sparsity coding is the efficiency with which multiplication and other matrix operations can be performed. This is best illustrated by a sample FORTRAN coded needed to multiply a matrix stored in this mode, by a vector $B(i)$:

```
DO I =1, N
      C(I) = DIAG(I) * B(I)
      DO J = IROW(I), IROW(I + 1) − 1
      C(I) = C(I) + OFFD(J) * B(ICOL(J))
      ENDDO
ENDDO
```

(23)

The above double loop involves $5N$ multiplications and $4N$ additions, without the need of search and compare operations. To perform the same operation using the brute force, full storage approach would require N^2 multiplications and N^2 additions. Thus, for a system of 1000 unknowns, the sparsity-based method is at least 200 times faster than the full storage approach in performing matrix multiplication.

To solve Eq. (20), [Y] can be inverted and the inverse multiplied by [V_0]. However, for sparse systems, complete matrix inversion should be avoided. The reason is that, in most cases, the inverse of a sparse matrix is full, for which the advantages of sparsity coding cannot be exploited. The solution of sparsity coded linear systems is typically obtained by using the LU decomposition, since usually the L and U factors are sparse. Note that the sparsity of the L and U factor matrices can be significantly affected by the ordering of the grid nodes (i.e., in which sequence [ϕ] was filled). Several very successful node ordering schemes that are associated with the analysis of electrical networks were reported for the solution of sparse matrix equations (see Ref. 16). Unfortunately, the grid node connectivity in typical FDM problems is such that the L and U factor matrices are considerably fuller than the original matrix [Y], even if the nodes are optimally ordered. Therefore, direct solution techniques are not as attractive for use in FDM as they are for large network problems.

Unlike the direct solution methods, there are iterative techniques for solving matrix equations, which do not require LU factoring. One of them is the Conjugate Gradient Method (17–19).

This method uses a sequence of matrix/vector multiplications, which can be performed very efficiently using the sparsity coding scheme described above.

Convergence. Given the FDM equations in matrix form, either direct (16) or iterative methods (17–19) such as the Conjugate Gradient Method (CGM) can be readily applied. It is important to point out that CGM-type algorithms are considerably faster than direct solution, provided that a good initial guess is used. One simple approach is to assume that the potential is zero everywhere, but on the surface of the conductor, and let this be an initial guess to start the CGM algorithm. For this initial guess, the convergence is very poor and the solution takes a long time. To improve the initial guess, several iterations of the SOR-based FDM algorithm can be performed to calculate the potential everywhere within the grid. It was found that for many practical problems, 10 to 15 iterations provide a very good initial guess for CGM.

From the performance point of view, the speed of CGM was most noticeable when compared to the SOR-based algorithm. In many problems, CGM was found to be an order of magnitude faster than SOR. In all fairness to SOR, its implementation, as described above, can be improved considerably by using the so-called multigrid/multilevel acceleration (20–21). The idea behind this method is to perform the iterations over coarse and fine grids alternatively, where the coarse grid points also coincide with and are a part of the fine grid. This means that iterations are first performed over a coarse grid, then interpolated to the fine grid and iterated over the fine grid. More complex multigrid schemes involve several layers of grids with different levels of discretization, with the iterations being performed interchangeably on all grids.

Finally, it should be pointed out that theoretical aspects of convergence for algorithms discussed thus far are well-documented and are outside the main scope of this article. The interested reader should consult Refs. 15, 18, or 19 for detailed mathematical treatment and assessment of convergence.

ADVANCED TOPICS

Open Boundary Truncation

If the electrostatic boundary-value problem consists of charged conductors in a region of infinite extent, then the simplest approach to truncate the computational (or FDM) boundary is with an equipotential wall of zero voltage. This has the advantage of being easy to implement, but leads to erroneous solution, especially if the truncation boundary is too close to the charged conductors. On the other hand, placing it too far from the region of interest may result in unacceptably large computational volume, which will require large computational resources.

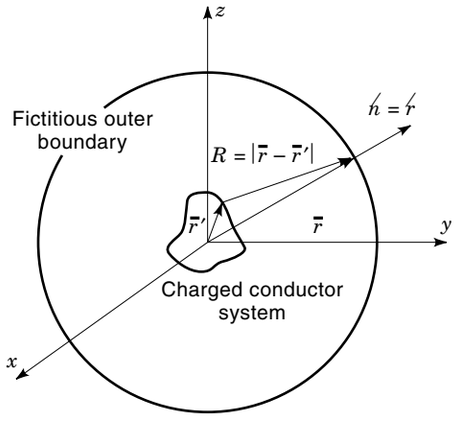

Figure 5. Virtual surface used for boundary truncation.

Although some early attempts to overcome such difficulties (5) provided the initial groundwork, rigorous absorbing boundary truncation operators were recently introduced (22–24) for dynamic problems, which can be modified for electrostatics. They are based on deriving mathematical operators that help simulate the behavior of the potential on a virtual boundary truncation surface, which is placed close to charged conductors (see Fig. 5). In essence, these operators provide the means for numerically approximating the proper behavior of the potential at infinity within a computational volume of finite extent.

Such absorbing boundary conditions (ABCs) are based on the fact that the potential due to any 3-D charge distribution is inversely proportional to the distance measured from it. Consider an arbitrary collection of charged conductors shown in Fig. 5. Although it is located in free unbounded space, a fictitious surface will be placed around it, totally enclosing all conductors. If this surface is far away from the charged conductor system—namely, if $\vec{r}$ is much greater that $\vec{r}'$—then the dominant radial variation of potential, ϕ, will be given by

$$\frac{1}{|\vec{r} - \vec{r}'|} \to \frac{1}{r} \tag{24}$$

If the fictitious boundary is moved closer toward the conductor assembly, then the potential will also include additional terms with higher inverse powers of r. These terms will contribute to the magnitude of the potential more significantly than those with lower inverse powers of r, as r becomes small.

The absorbing boundary conditions emphasize the effect of leading (dominant) radial terms on the magnitude of the potential evaluated on the fictitious (boundary truncation) surface. The ABCs provide the proper analytic means to annihilate the nonessential terms, instead of simply neglecting their contribution. Numerically, this can be achieved by using the so-called absorbing boundary truncation operators.

In general, absorbing boundary operators can be of any order. For example, as shown in Ref. 23, the first- and second-order operators in 3-D have the following forms:

$$B_1 u = \frac{\partial u}{\partial r} + \frac{u}{r} = O\left(\frac{1}{r^3}\right) \to 0 \qquad \text{as } r \to \infty \tag{25}$$

$$B_2 u = \left(\frac{\partial}{\partial r} + \frac{3}{r}\right)\left(\frac{\partial u}{\partial r} + \frac{u}{r}\right) = O\left(\frac{1}{r^5}\right) \to 0 \qquad \text{as } r \to \infty \tag{26}$$

where u is the scalar electric potential function, ϕ, that satisfies the Laplace equation, and $r = |\vec{r}|$ is the radial distance measured from the coordinate origin (see Fig. 5). Since FDM is based on the iterative solution to the Laplace equation, small increases in the overall lattice (discretized 3-D space whose planes are 2-D grids) size do not slow the algorithm down significantly, nor do they require an excessive amount of additional computer memory. As a result, from a practical standpoint, the fictitious boundary truncation surface need not be placed too close to the region of interest, therefore not requiring the use of high-order ABC operators in order to simulate proper behavior of the potential at lattice boundaries accurately. Consequently, in practice, it is sufficient to use the first-order operator, B_1, to model open boundaries. Previous numerical studies suggest that this choice is indeed adequate for many engineering problems (25).

To be useful for geometries that mostly conform to rectangular coordinates, the absorption operator B_1, when expressed in Cartesian coordinates, takes on the following form:

$$\frac{\partial u}{\partial x} \approx \mp\left(\frac{u}{x} + \frac{y}{x}\frac{\partial u}{\partial y} + \frac{z}{x}\frac{\partial u}{\partial z}\right) \tag{27}$$

$$\frac{\partial u}{\partial y} \approx \mp\left(\frac{u}{y} + \frac{x}{y}\frac{\partial u}{\partial x} + \frac{z}{y}\frac{\partial u}{\partial z}\right) \tag{28}$$

$$\frac{\partial u}{\partial z} \approx \mp\left(\frac{u}{z} + \frac{x}{z}\frac{\partial u}{\partial x} + \frac{y}{z}\frac{\partial u}{\partial y}\right) \tag{29}$$

where $\mp$ signs correspond to the outward pointing unit normal vectors $\hat{n} = \pm(\hat{x}, \hat{y}, \hat{z})$ for operators in Eqs. (27), (28), and (29), respectively.

The finite-difference approximations to the above equations which have been employed in the open boundary FDM algorithm are given by

$$u_{i+1,j,k} = u_{i-1,j,k} - \frac{(h_i + h_{i-1})}{(x_{i,j,k} - x_{\text{ref}})} \left[u_{i,j,k} + \frac{(y_{i,j,k} - y_{\text{ref}})(u_{i,j+1,k} - u_{i,j-1,k})}{(h_j + h_{j-1})} + \frac{(z_{i,j,k} - z_{\text{ref}})(u_{i,j,k+1} - u_{i,j,k-1})}{(h_k + h_{k-1})}\right] \tag{30}$$

$$u_{i,j+1,k} = u_{i,j-1,k} - \frac{(h_j + h_{j-1})}{(y_{i,j,k} - y_{\text{ref}})} \left[u_{i,j,k} + \frac{(x_{i,j,k} - x_{\text{ref}})(u_{i+1,j,k} - u_{i-1,j,k})}{(h_i + h_{i-1})} + \frac{(z_{i,j,k} - z_{\text{ref}})(u_{i,j,k+1} - u_{i,j,k-1})}{(h_k + h_{k-1})}\right] \tag{31}$$

$$u_{i,j,k+1} = u_{i,j,k-1} - \frac{(h_k + h_{k-1})}{(z_{i,j,k} - z_{\text{ref}})} \left[u_{i,j,k} + \frac{(x_{i,j,k} - x_{\text{ref}})(u_{i+1,j,k} - u_{i-1,j,k})}{(h_i + h_{i-1})} + \frac{(y_{i,j,k} - y_{\text{ref}})(u_{i,j+1,k} - u_{i,j-1,k})}{(h_j + h_{j-1})}\right] \tag{32}$$

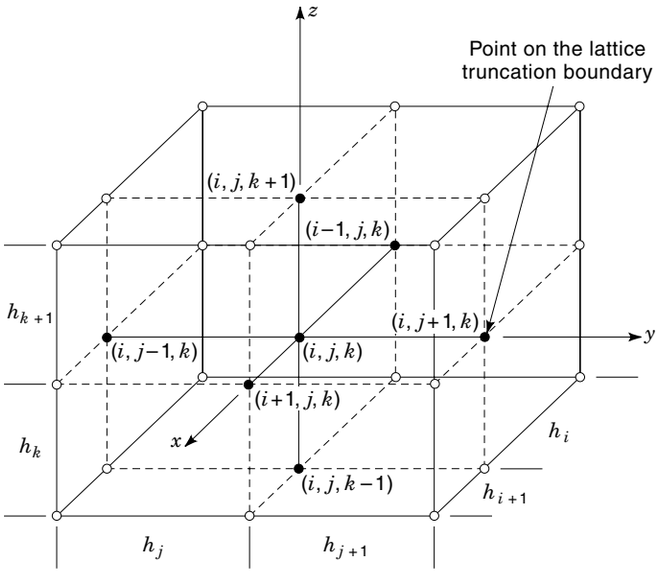

Figure 6. Detail of FDM lattice near the boundary truncation surface.

where $(x, y, z)_{\text{ref}}$ are the x, y, and z components of a vector pointing (referring) to the geometric center of the charged conductor assembly, with other quantities that appear in Eqs. (30) through (32) shown in Fig. 6. It is important to add that the $(x, y, z)_{i,j,k} - (x, y, z)_{\text{ref}}$ terms are the x, y, and z components of a vector from the truncation boundary to the geometrical center of the charged conductor system.

Notice that Fig. 6 graphically illustrates the FDM implementation of the open boundary truncation on lattice faces aligned along the xz plane. On this plane, the normal is in the y direction, for which Eq. (31) is the FDM equivalent of the first-order absorbing boundary operator in Cartesian coordinates. Similarly, Eqs. (32) and (30) are used to simulate the open boundary on xy and yz faces of the lattice, respectively.

When reduced to two dimensions, the absorption operator, B_1, in Cartesian coordinates, takes on the form given below:

$$\frac{\partial u}{\partial x} \approx \mp\left(\frac{1}{x} + \frac{y}{x}\frac{\partial u}{\partial y}\right) \tag{33}$$

$$\frac{\partial u}{\partial y} \approx \mp\left(\frac{1}{y} + \frac{\partial u}{\partial x}\right) \tag{34}$$

The discrete versions of the above equations can be written as

$$u_{i+1,j} = \mp\left\{u_{i-1,j} - \frac{(h_i + h_{i-1})}{(x_{i,j} - x_{\text{ref}})}\left[u_{i,j} + \frac{(y_{i,j} - y_{\text{ref}})(u_{i,j+1} - u_{i,j-1})}{(h_j + h_{j-1})}\right]\right\} \tag{35a}$$

$$u_{i,j+1} = \mp\left\{u_{i,j-1} - \frac{(h_j + h_{j-1})}{(y_{i,j} - y_{\text{ref}})}\left[u_{i,j} + \frac{(x_{i,j} - x_{\text{ref}})(u_{i+1,j} - u_{i-1,j})}{(h_i + h_{i-1})}\right]\right\} \tag{35b}$$

where, as before, $\mp$ correspond to the outward pointing unit normal vectors $\hat{n} = \pm(\hat{x}, \hat{y})$ for operators in Eqs. (33) and (34) or (35a) and (35b), respectively. The points $x_{i,j}$ and $y_{i,j}$ denote those points in the grid that are located one cell away from the truncation boundary, while x_{ref} and y_{ref} correspond to the center of the cylinder in Figs. 2 and 4.

Finally, another approach to open boundary truncation, which is worth mentioning, involves the regular finite-difference scheme supplemented by the use of electrostatic surface equivalence (26). A virtual surface S_v is defined near the actual grid truncation boundary. The electrostatic potential due to charged objects, enclosed within S_v, is computed using the regular FDM algorithm. Subsequently, it is used to calculate the surface charge density and surface magnetic current, which are proportional to the normal and tangential components of the electric field on S_v.

Once the equivalent sources are known, the potential between the virtual surface and the grid truncation boundary can be readily calculated (for details see Ref. 26). This procedure is repeated every iteration, and since the potential on the virtual surface is estimated correctly, it produces a physical value of the potential on the truncation boundary. As demonstrated in Ref. 26, this approach leads to very accurate results in boundary-value problems with charged conductors embedded in open regions.

It is vastly superior to simply using the grounded conductor to terminate the computational space.

Inclusion of Dielectric Anisotropy

Network Analog Approach. Many materials such as printed circuit board and microwave circuit substrates, which are commonly used in electrical engineering exhibit anisotropic behavior. The electrical properties of these materials vary with direction and have to be described by a tensor instead of a single scalar quantity. This section will examine how the anisotropy affects the FDM and how the algorithnm must be changed to accommodate the solution of 3-D problems containing such materials. The theoretical development presented below is a generalization of that available in Ref. 27 and is restricted to linear anisotropic dielectrics only.

In an attempt to provide a more intuitive interpretation to the abstract nature of the FDM algorithm, an equivalent circuit model will be used for linear inhomogeneous, anisotropic regions. This approach is called *resistance network analog* (6). It was initially proposed for approximating the solution of the Laplace equation in two dimensions experimentally, with a network of physical resistors whose values could be adjusted to correspond to the weighting factors [e.g., the Y's in Eq. (7)] that appear in the FDM algorithm. Since its introduction, the resistance network approach has been implemented numerically in the analysis of (a) homogeneous dielectrics in 3-D (28) and (b) simple biaxial anisotropic materials (described by diagonal permitivitty tensors) in 2-D (29).

Since the resistance network analog gives a physical intepretation to FDM, the discretized versions of the Laplace equations for anisotropic media will be recast into this form. As the details of FDM were described earlier, only the key steps in developing the two-dimensional model are summarized below. Moreover, for the sake of brevity, the discussion of the three-dimensional case will be limited to the final equations and their pictorial interpretation.

The Laplace equation for boundary-value problems involving inhomogeneous and anisotropic dielectrics in three-dimensions is given by

$$\nabla \cdot (\epsilon_0[\epsilon_r(x,y,z)] \cdot \nabla\phi(x,y,z)) = 0 \tag{36}$$

In the above equation, $[\epsilon_r]$ stands for the relative dielectric tensor and is defined as

$$[\epsilon] = \begin{bmatrix} \epsilon_{xx} & \epsilon_{xy} & \epsilon_{xz} \\ \epsilon_{yx} & \epsilon_{yy} & \epsilon_{yz} \\ \epsilon_{zx} & \epsilon_{zy} & \epsilon_{zz} \end{bmatrix} \tag{37}$$

Since the material properties need not be homogeneous in the region of interest, the elements of $[\epsilon_r]$ are assumed to be functions of position. The dielectric is assumed to occupy only part of the modeling (computational) space, and its properties may vary from point to point. When Eq. (37) is substituted into Eq. (36) and rewritten in a matrix form as

$$\left[\frac{\partial}{\partial x}\frac{\partial}{\partial y}\frac{\partial}{\partial z}\right] \cdot \begin{bmatrix} \epsilon_{xx}\dfrac{\partial\phi}{\partial x} + \epsilon_{xy}\dfrac{\partial\phi}{\partial y} + \epsilon_{xz}\dfrac{\partial\phi}{\partial z} \\ \epsilon_{yx}\dfrac{\partial\phi}{\partial x} + \epsilon_{yy}\dfrac{\partial\phi}{\partial y} + \epsilon_{yz}\dfrac{\partial\phi}{\partial z} \\ \epsilon_{zx}\dfrac{\partial\phi}{\partial x} + \epsilon_{zy}\dfrac{\partial\phi}{\partial y} + \epsilon_{zz}\dfrac{\partial\phi}{\partial z} \end{bmatrix} = 0 \tag{38}$$

it provides the starting point for developing the corresponding FDM algorithm.

After eliminating the z-dependent terms and fully expanding the above equation by following the notation used throughout this paper, the finite-difference approximation for the potential at every nodal point in a 2-D grid is given by

$$\phi_{i,j}^{p+1} = (1-\Omega)\phi_{i,j}^{p} + \frac{\Omega}{Y_{i,j}} \times \left\{ \begin{array}{l} (\phi_{i+1,j}^{p} Y_{i+1}\phi_{i-1,j}^{p+1} Y_{i-1}) \\ +(\phi_{i,j+1}^{p} Y_{j+1} + \phi_{i,j-1}^{p+1} Y_{j-1}) \\ +(\phi_{i+1,j+1}^{p} Y_{i+1,j+1} + \phi_{i-1,j-1}^{p+1} Y_{i-1,j-1}) \\ -(\phi_{i-1,j+1}^{p} Y_{i-1,j+1} + \phi_{i+1,j-1}^{p+1} Y_{i+1,j-1}) \end{array} \right\} \tag{39}$$

where

$$Y_{i\pm1} = \begin{pmatrix} (\epsilon_{i,j-1}^{yy} + \epsilon_{i,j}^{yy}) \\ (\epsilon_{i-1,j-1}^{yy} + \epsilon_{i-1,j}^{yy}) \end{pmatrix} \left(\frac{1}{h_i} + \frac{2}{h_i + h_{i-1}}\right) + \left(\frac{2}{h_i + h_{i-1}}\right)\left(\frac{2}{h_j + h_{j-1}}\right)\left[\left(\epsilon_{i,j}^{zy} + \epsilon_{i-1,j}^{zy}\right) - \left(\epsilon_{i-1,j-1}^{zy} + \epsilon_{i,j-1}^{zy}\right)\right] \tag{40}$$

$$Y_{j\pm1} = \begin{pmatrix} (\epsilon_{i-1,j}^{zz} + \epsilon_{i,j}^{zz}) \\ (e_{i-1,j-1}^{zz} + \epsilon_{i,j-1}^{zz}) \end{pmatrix} \left(\frac{1}{h_j} + \frac{2}{h_j + h_{j-1}}\right) + \left(\frac{2}{h_i + h_{i-1}}\right)\left(\frac{2}{h_j + h_{j-1}}\right)\left[\left(\epsilon_{i,j-1}^{yz} + \epsilon_{i,j}^{yz}\right) - \left(\epsilon_{i-1,j-1}^{yz} + \epsilon_{i-1,j}^{yz}\right)\right] \tag{41}$$

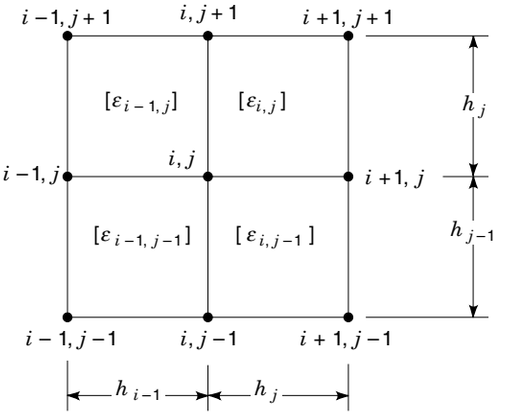

Figure 7. Detail with FDM cell for anisotropic medium in two dimensions.

$$Y_{i\pm1,j\pm1} = Y_{i\pm1,j\mp1} = \left(\frac{2}{h_i + h_{i-1}}\right)\left(\frac{2}{h_j + h_{j-1}}\right) \left[\epsilon_{i,j}^{yz} + \epsilon_{i-1,j}^{yz} + \epsilon_{i-1,j-1}^{yz} + \epsilon_{i,j-1}^{yz} + \epsilon_{i,j}^{zy} + \epsilon_{i-1,j}^{zy} + \epsilon_{i-1,j-1}^{zy} + \epsilon_{i,j-1}^{zy}\right] \tag{42}$$

$$Y_{i,j} = Y_{i+1} + Y_{i-1} + Y_{j+1} + Y_{j-1} \tag{43}$$

Note that unlike the treatment of isotropic dielectrics, the permittivity of each cell is now described by a tensor (see Fig. 7). In addition, the presence of the anisotropy is responsible for added coupling between the voltage $\phi_{i,j}$ and voltages $\phi_{i\pm1,j\pm1}$ (actually all four combinations of the subscripts).

The symbols Y in Eq. (39) can be interpreted as admittances representing the "electrical link" between the grid point voltages. The resulting equivalent network for Eq. (39) can thus be represented pictorially as shown in Fig. 8.

Similarly, after fully expanding Eq. (36) in three dimensions, the following finite-difference approximation for the potential at every nodal point in a 3-D lattice can be obtained:

$$\phi_{i,j,k}^{p+I} = (1-\Omega)\phi_{i,j,k}^{p} + \frac{\Omega\phi_{\text{new}}}{Y_{i,j,k}} \tag{44}$$

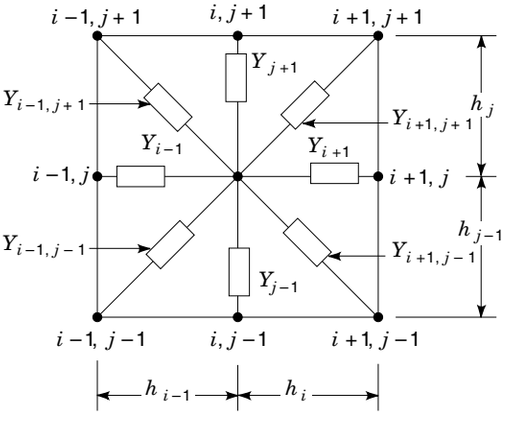

Figure 8. Network analog for 2-D FDM algorithm at grid point i, j for arbitrary anisotropic medium.

where ϕ_{new} is defined as

$$\begin{aligned}\phi_{\text{new}} = {} & \phi^p_{i+1,j,k}\left(Y_{i+1}+Y^A_1\right)+\phi^{p-1}_{i-1,j,k}\left(Y_{i-1}-Y^A_1\right)\\ & +\phi^p_{i,j+1,k}\left(Y_{j+1}+Y^A_2\right)+\phi^{p-1}_{i,j-1,k}\left(Y_{j-1}-Y^A_2\right)\\ & +\phi^p_{i,j,k+1}\left(Y_{k+1}+Y^A_3\right)+\phi^{p-1}_{i,j,k-1}\left(Y_{k-1}-Y^A_3\right)\\ & +Y^A_4\left[\left(\phi^p_{i+1,j+1,k}-\phi^{p-1}_{i-1,j-1,k}\right)-\left(\phi^p_{i-1,j+1,k}+\phi^p_{i+1,j-1,k}\right)\right]\\ & +Y^A_5\left[\left(\phi^p_{i+1,j,k+1}+\phi^{p-1}_{i-1,j,k-1}\right)-\left(\phi^p_{i-1,j,k+1}+\phi^p_{i+1,j,k-1}\right)\right]\\ & +Y^A_6\left[\left(\phi^p_{i,j+1,k+1}+\phi^{p-1}_{i,j-1,k-1}\right)-\left(\phi^p_{i,j+1,k-1}+\phi^p_{i,j-1,k+1}\right)\right]\end{aligned} \tag{45}$$

and

$$Y_{i,j,k} = Y_{i+1}+Y_{i-1}+Y_{j+1}+Y_{j-1}+Y_{k-1}+Y_{k+1}$$

The Y terms appearing in Eqs. (44) and (45) are given by

$$Y_{i-1} = \frac{2}{h_i+h_{i-1}}\left[T_{1,xx}\left(\frac{1}{h_{i-1}}-\frac{2}{h_i+h_{i-1}}\right)+T_{2,xx}\left(\frac{1}{h_{i-1}}+\frac{2}{h_i+h_{i-1}}\right)\right] \tag{46}$$

$$Y_{i+1} = \frac{2}{h_i+h_{i-1}}\left[T_{1,xx}\left(\frac{1}{h_i}+\frac{2}{h_i+h_{i-1}}\right)+T_{2,xx}\left(\frac{1}{h_i}+\frac{2}{h_i+h_{i-1}}\right)\right] \tag{47}$$

$$Y_{j-1} = \frac{2}{h_j+h_{j-1}}\left[T_{1,yy}\left(\frac{1}{h_{j-1}}-\frac{2}{h_j+h_{j-1}}\right)+T_{2,yy}\left(\frac{1}{h_{j-1}}+\frac{2}{h_j+h_{j-1}}\right)\right] \tag{48}$$

$$Y_{j+1} = \frac{2}{h_j+h_{j-1}}\left[T_{1,yy}\left(\frac{1}{h_j}+\frac{2}{h_j+h_{j-1}}\right)+T_{2,yy}\left(\frac{1}{h_j}-\frac{2}{h_j+h_{j-1}}\right)\right] \tag{49}$$

$$Y_{k-1} = \frac{2}{h_k+h_{k-1}}\left[T_{1,zz}\left(\frac{1}{h_{k-1}}-\frac{2}{h_k+h_{k-1}}\right)+T_{2,zz}\left(\frac{1}{h_{k-1}}+\frac{2}{h_k+h_{k-1}}\right)\right] \tag{50}$$

$$Y^A_1 = \left(\frac{2}{h_j+h_{j-1}}\right)\left(\frac{2}{h_i+h_{i-1}}\right)(T_{1,yx}-T_{2,yx})+\left(\frac{2}{h_k+h_{k-1}}\right)\left(\frac{2}{h_i+h_{i-1}}\right)(T_{1,zx}-T_{2,zx}) \tag{51}$$

$$Y^A_2 = \left(\frac{2}{h_j+h_{j-1}}\right)\left(\frac{2}{h_i+h_{i-1}}\right)(T_{1,xy}-T_{2,xy})+\left(\frac{2}{h_k+h_{k-1}}\right)\left(\frac{2}{h_j+h_{j-1}}\right)(T_{1,zy}-T_{2,zy}) \tag{52}$$

$$Y^A_3 = \left(\frac{2}{h_k+h_{k-1}}\right)\left(\frac{2}{h_i+h_{i-1}}\right)(T_{1,xz}-T_{2,xz})+\left(\frac{2}{h_k+h_{k-1}}\right)\left(\frac{2}{h_j+h_{j-1}}\right)(T_{1,yz}-T_{2,yz}) \tag{53}$$

$$Y^A_4 = 2\left(\frac{2}{h_j+h_{j-1}}\right)\left(\frac{2}{h_i+h_{i-1}}\right)\left(\frac{T_{1,xy}+T_{2,xy}}{8}+\frac{T_{1,yx}+T_{2,yx}}{8}\right) \tag{54}$$

$$Y^A_5 = 2\left(\frac{2}{h_k+h_{k-1}}\right)\left(\frac{2}{h_i+h_{i-1}}\right)\left(\frac{T_{1,xz}+T_{2,xz}}{8}+\frac{T_{1,zx}+T_{2,zx}}{8}\right) \tag{55}$$

$$Y^A_6 = 2\left(\frac{2}{h_j+h_{j-1}}\right)\left(\frac{2}{h_k+h_{k-1}}\right)\left(\frac{T_{1,yz}+T_{2,yz}}{8}+\frac{T_{1,zy}+T_{2,zy}}{8}\right) \tag{56}$$

with the T terms having the following forms:

$$T_{1,xx} = \epsilon^{xx}_{i,j-1,k-1}+\epsilon^{xx}_{i,j,k-1}+\epsilon^{xx}_{i,j-1,k}+\epsilon^{xx}_{i,j,k} \tag{57a}$$

$$T_{2,xx} = \epsilon^{xx}_{i-1,j-1,k-1}+\epsilon^{xx}_{i-1,j,k-1}+\epsilon^{xx}_{i-1,j-1,k}+\epsilon^{xx}_{i-1,j,k} \tag{57b}$$

$$T_{1,yy} = \epsilon^{yy}_{i-1,j,k-1}+\epsilon^{yy}_{i,j,k-1}+\epsilon^{yy}_{i-1,j,k}+\epsilon^{yy}_{i,j,k} \tag{58a}$$

$$T_{2,yy} = \epsilon^{yy}_{i-1,j-1,k-1}+\epsilon^{yy}_{i,j-1,k-1}+\epsilon^{yy}_{i-1,j-1,k}+\epsilon^{yy}_{i,j-1,k} \tag{58b}$$

$$T_{1,zz} = \epsilon^{zz}_{i-1,j-1,k}+\epsilon^{zz}_{i,j-1,k}+\epsilon^{zz}_{i-1,j,k}+\epsilon^{zz}_{i,j,k} \tag{59a}$$

$$T_{2,zz} = \epsilon^{zz}_{i-1,j-1,k-1}+\epsilon^{zz}_{i,j-1,k-1}+\epsilon^{zz}_{i-1,j,k-1}+\epsilon^{zz}_{i,j,k-1} \tag{59b}$$

$$T_{1,xy} = \epsilon^{xy}_{i,j-1,k-1}+\epsilon^{xy}_{i,j,k-1}+\epsilon^{xy}_{i,j-1,k}+\epsilon^{xy}_{i,j,k} \tag{60a}$$

$$T_{2,xy} = \epsilon^{xy}_{i-1,j-1,k-1}+\epsilon^{xy}_{i-1,j,k-1}+\epsilon^{xy}_{i-1,j-1,k}+\epsilon^{xy}_{i-1,j,k} \tag{60b}$$

$$T_{1,xz} = \epsilon^{xz}_{i,j-1,k-1}+\epsilon^{xz}_{i,j,k-1}+\epsilon^{xz}_{i,j-1,k}+\epsilon^{xz}_{i,j,k} \tag{61a}$$

$$T_{2,xz} = \epsilon^{xz}_{i-1,j-1,k-1}+\epsilon^{xz}_{i-1,j,k-1}+\epsilon^{xz}_{i-1,j-1,k}+\epsilon^{xz}_{i-1,j,k} \tag{61b}$$

$$T_{1,yx} = \epsilon^{yx}_{i-1,j,k-1}+\epsilon^{yx}_{i,j,k-1}+\epsilon^{yx}_{i-1,j,k}+\epsilon^{yx}_{i,j,k} \tag{62a}$$

$$T_{2,yx} = \epsilon^{yx}_{i-1,j-1,k-1}+\epsilon^{yx}_{i,j,-1,k-1}+\epsilon^{yx}_{i-1,j-1,k}+\epsilon^{yx}_{i,j-1,k} \tag{62b}$$

$$T_{1,yz} = \epsilon^{yz}_{i-1,j,k-1}+\epsilon^{yz}_{i,j,k-1}+\epsilon^{yz}_{i-1,j,k}+\epsilon^{yz}_{i,j,k} \tag{63a}$$

$$T_{2,yz} = \epsilon^{yz}_{i-1,j-1,k-1}+\epsilon^{yz}_{i,j-1,k-1}+\epsilon^{yz}_{i-1,j-1,k}+\epsilon^{yz}_{i,j-1,k} \tag{63b}$$

$$T_{1,zx} = \epsilon^{zx}_{i-1,j-1,k}+\epsilon^{zx}_{i,j-1,k}+\epsilon^{zx}_{i-1,j,k}+\epsilon^{zx}_{i,j,k} \tag{64a}$$

$$T_{2,zx} = \epsilon^{zx}_{i-1,j-1,k-1}+\epsilon^{zx}_{i,j-1,k-1}+\epsilon^{zx}_{i-1,j,k-1}+\epsilon^{zx}_{i,j,k-1} \tag{64b}$$

$$T_{1,zy} = \epsilon^{zy}_{i-1,j-1,k}+\epsilon^{zy}_{i,j-1,k}+\epsilon^{zy}_{i-1,j,k}+\epsilon^{zy}_{i,j,k} \tag{65a}$$

$$T_{2,zy} = \epsilon^{zy}_{i-1,j-1,k-1}+\epsilon^{zy}_{i,j-1,k-1}+\epsilon^{zy}_{i-1,j,k-1}+\epsilon^{zy}_{i,j,k-1} \tag{65b}$$

Note that Eq. (45) has a similar interpretation as its 2-D counterpart Eq. (39). It can also be represented by an equivalent network, whose diagonal terms are shown in Fig. 9. For clarity, the off-diagonal terms, which provide the connections of $\phi_{i,j,k}$ to the voltages at the remaining nodes in Eq. (45), are shown separately in Fig. 10.

Coordinate Transformation Approach. Coordinate transformations can be used to simplify the solution to electrostatic boundary-value problems. Such transformations can reduce the complexity arising from complicated geometry or from the presence of anisotropic materials. In general, these methods utilize coordinate transformation to map complex geometries or material properties into simpler ones, through a specific relationship which links each point in the original and transformed problems, respectively.

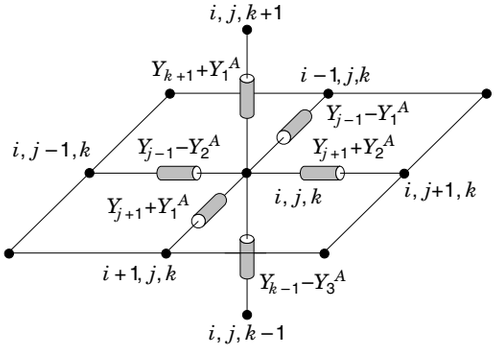

Figure 9. Network analog for 3-D FDM algorithm at grid point i, j for anisotropic dielectric with diagonal permittivity tensor.

One class of coordinate transformations, known as *conformal mapping,* is based on modifying the original complex geometry to one for which an analytic solution is available. This technique requires extensive mathematical expertise in order to identify an appropriate coordinate transformation function. Its applications are limited to a few specific geometrical shapes for which such functions exist. Furthermore, the applications are restricted to two-dimensional problems. Even though this technique can be very powerful, it is usually rather tedious and thus it is considered beyond the scope of this article. The interested reader can refer to Ref. 30, among others, for further details.

The second class of coordinate transformations reduces the complexity of the FDM formulation in problems involving anisotropic materials. As described in the previous section, the discretization of the Laplace equation in anisotropic regions [Eq. (36)] is considerably more complicated than the corresponding procedure for isotropic media [Eq. (7)]. However, it can be shown that a sequence of rotation and scaling transformations can convert any symmetric permittivity tensor into an identity matrix (i.e., free space). As a result, the FDM solution of the Laplace equation in the transformed coordinate system is considerably simplified, since the anisotropic dielectric is eliminated.

To illustrate the concept, this technique will be demonstrated with two-dimensional examples. In 2-D (no z dependence is assumed) the Laplace equation can be written as

$$\nabla \cdot ([\epsilon_r(x, y)]\nabla\phi) = 0 \tag{66}$$

where

$$[\epsilon_r] = \begin{bmatrix} \epsilon_{xx} & \epsilon_{xy} \\ \epsilon_{yx} & \epsilon_{yy} \end{bmatrix} \tag{67}$$

If the principal (crystal or major) axes of the dielectric are aligned with the coordinate system of the geometry, then the off-diagonal terms vanish. Otherwise, $[\epsilon_r]$ is a full symmetric matrix. In this case, any linear coordinate transformation of the form

$$\begin{bmatrix} x' \\ y' \end{bmatrix} = [A] \begin{bmatrix} x \\ y \end{bmatrix} \tag{68}$$

(where $[A]$ is a 2×2 nonsingular matrix of constant coefficients) also transforms the permittivity tensor as follows:

$$[\epsilon'] = [A]^{-1}[\epsilon_r][A] \tag{69}$$

Next, consider the structure shown in Fig. 11(a). It consists of a perfect conductor (metal) embedded in an anisotropic dielectric, all enclosed within a rectangular conducting shell. The field within the rectangular shell must be determined given the potentials on all conductors. In this example, $[\epsilon_r]$ is assumed to be diagonal:

$$[\epsilon_r] = \begin{bmatrix} \epsilon_{xx} & 0 \\ 0 & \epsilon_{yy} \end{bmatrix} \tag{70}$$

By scaling the coordinates with

$$[A] = \begin{bmatrix} 1/\sqrt{\epsilon_{xx}} & 0 \\ 0 & 1/\sqrt{\epsilon_{yy}} \end{bmatrix} \tag{71}$$

the permittivity can be transformed into an identity matrix. The geometry of the structure is deformed as shown in Fig. 11(b), with the corresponding rectangular discretization grid depicted in Fig. 11(c). Note that the locations of the unknown potential variables are marked by white dots, while the conducting boundaries are represented by known potentials and their locations are denoted by black dots. The potential in the transformed boundary-value problem can now be computed by applying the FDM algorithm, which is specialized for free space, since $[\epsilon_r]$ is an identity matrix.

Once the potential is computed everywhere, other quantities of interest, such as the E field and charge, can be calculated next. However, to correctly evaluate the required space derivatives, transformation back to original coordinates is required, as illustrated in Fig. 11(d). Note that in spite of the resulting simplifications, this method is limited to cases where the entire computational space is occupied by a single homogeneous anisotropic dielectric.

In general, when the principal (or major) axes of the permittivity are arbitrarily orientated with respect to the coordinate axes of the geometry, $[\epsilon_r]$ is a full symmetric matrix. In this case, $[\epsilon_r]$ can be diagonalized by an orthonormal coordi-

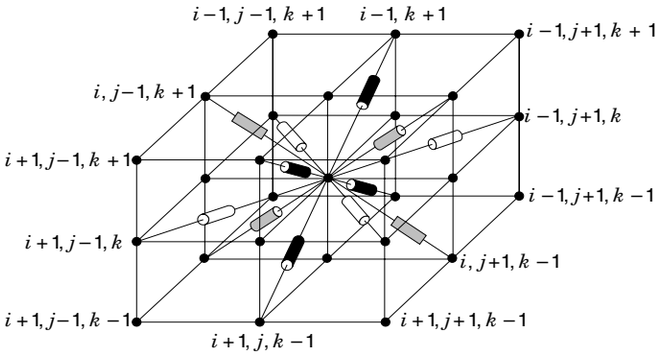

Figure 10. Network analog for 3-D FDM algorithm at grid point i, j for arbitrary anisotropic dielectric.

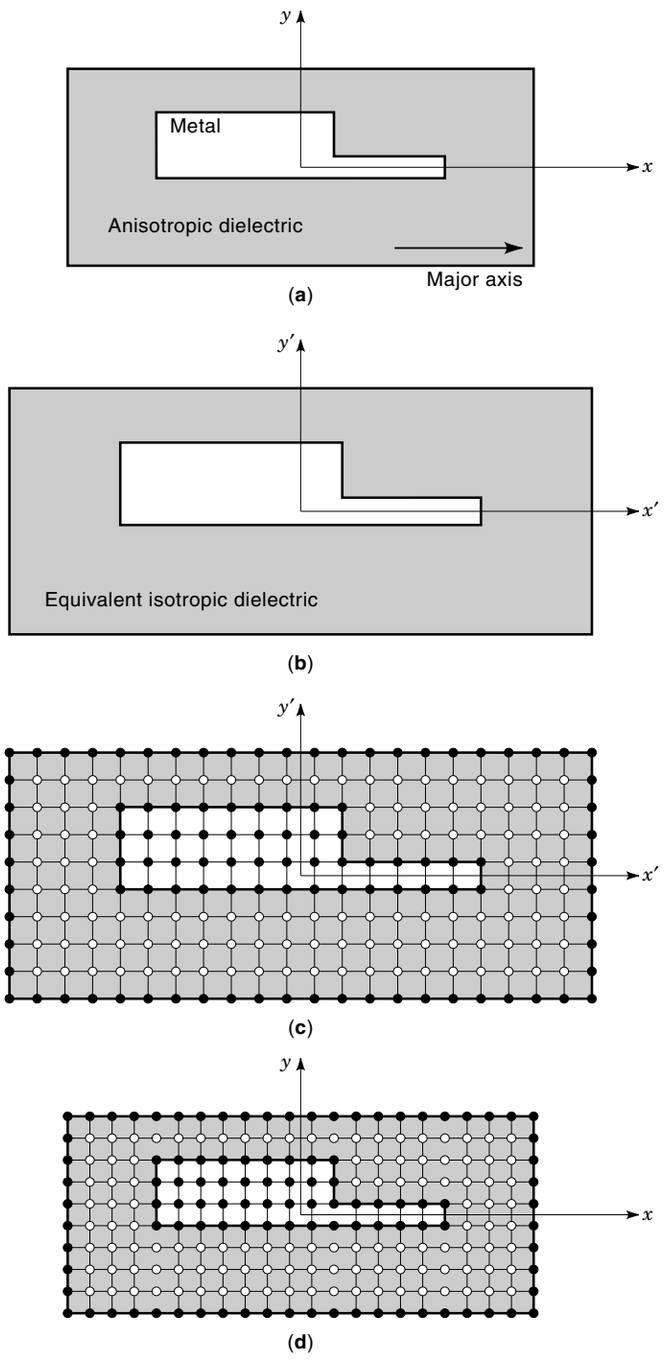

Figure 11. Graphical representation of coordinate transformation for homogeneous anisotropic dielectric with diagonal permittivity tensor.

nate transformation. Specifically, there exists a rotation matrix of the form:

$$[A] = \begin{bmatrix} \cos\theta & -\sin\theta \\ \sin\theta & \cos\theta \end{bmatrix} \tag{72}$$

such that the product,

$$[\epsilon'] = [A]^T[\epsilon_r][A] \tag{73}$$

is a diagonal matrix. The angle θ is defined as the angle by which the coordinate system should be rotated to align it with the major axes of the dielectric.

Consider the structure shown in Fig. 12(a), which is enclosed in a metallic shell. However, in this example the nonconducting region of interest includes both free space and an anisotropic dielectric. Furthermore, the major axis of $[\epsilon_r]$ is at 30 degrees with respect to that of the structure. The effect of rotating the coordinates by $\theta = -30$ degrees leads to a geometry shown in Fig. 12(b). In the transformed coordinate system, the major axis of the permittivity is horizontal and $[\epsilon_r]$ is a diagonal matrix. Observe that this transformation does not affect the dielectric properties of the free-space region (or of any other isotropic dielectrics, if present). However, the subsequent scaling operation for transforming the properties of the anisotropic region to free space is not useful. Such transformation also changes the properties of the original free-space region to those exhibiting anisotropic characteristics. Regardless of this limitation, the coordinate rotation alone considerably simplifies the FDM algorithm of Eq. (45) to

$$\begin{aligned} \phi_{\text{new}} = {} & \phi^p_{i+1,j,k}\left(Y_{i+1} + Y^A_1\right) + \phi^{p-1}_{i-1,j,k}\left(Y_{i-1} - Y^A_1\right) \\ & + \phi^p_{i,j+1,k}\left(Y_{j+1} + Y^A_2\right) + \phi^{p-1}_{i,j-1,k}\left(Y_{j-1} - Y^A_2\right) \end{aligned} \tag{74}$$

where all z-dependent (or k) terms have been removed.

Without the rotation, the permittivity is characterized by Eq. (67). Under such conditions, the corresponding FDM update equation includes four additional potential variables, as shown below:

$$\begin{aligned} \phi_{\text{new}} = {} & \phi^p_{i+1,j,k}\left(Y_{i+1} + Y^A_1\right) + \phi^{p-1}_{i-1,j,k}\left(Y_{i-1} - Y^A_1\right) \\ & + \phi^p_{i,j+1,k}\left(Y_{j+1} + Y^A_2\right) + \phi^{p-1}_{i,j-1,k}\left(Y_{j-1} - Y^A_2\right) \\ & + Y^A_4\left[\left(\phi^p_{i+1,j+1,k} - \phi^{p-1}_{i-1,j-1,k}\right)\right. \\ & \left. - \left(\phi^p_{i-1,j+1,k} + \phi^p_{i+1,j-1,k}\right)\right] \end{aligned} \tag{75}$$

The simplification resulting from coordinate rotation in three dimensions is even more significant. In the general case, the full FDM algorithm [Eq. (45)] contains 18 terms, while in the rotated coordinates the new equation has only 6.

Next, a rectangular discretization grid is constructed for the transformed geometry as shown in Fig. 12(c), with the unknown potential represented by white dots and conducting boundaries denoted by black dots. As can be seen, the rotation complicates the assignment (or definition) of the boundary nodes. In general, a finer discretization may be required to approximate the metal boundaries more accurately.

Once the potential field is computed, the transformation back to the original coordinates is performed by applying the inverse rotation $[A]^T$, as illustrated in Fig. 11(d). Note that in the original coordinate system, the grid is rotated and, as such, complicates the computation of electric field. In addition to the required coordinate mapping, this method is also limited to boundary-value problems containing only one type of anisotropic dielectric, though any number of isotropic dielectric regions may be present.

The above examples illustrate that coordinate transformations are beneficial in solving a narrow class of electrostatic problems. Undoubtedly, considerable computational savings can be achieved in the calculation of the potential using FDM.

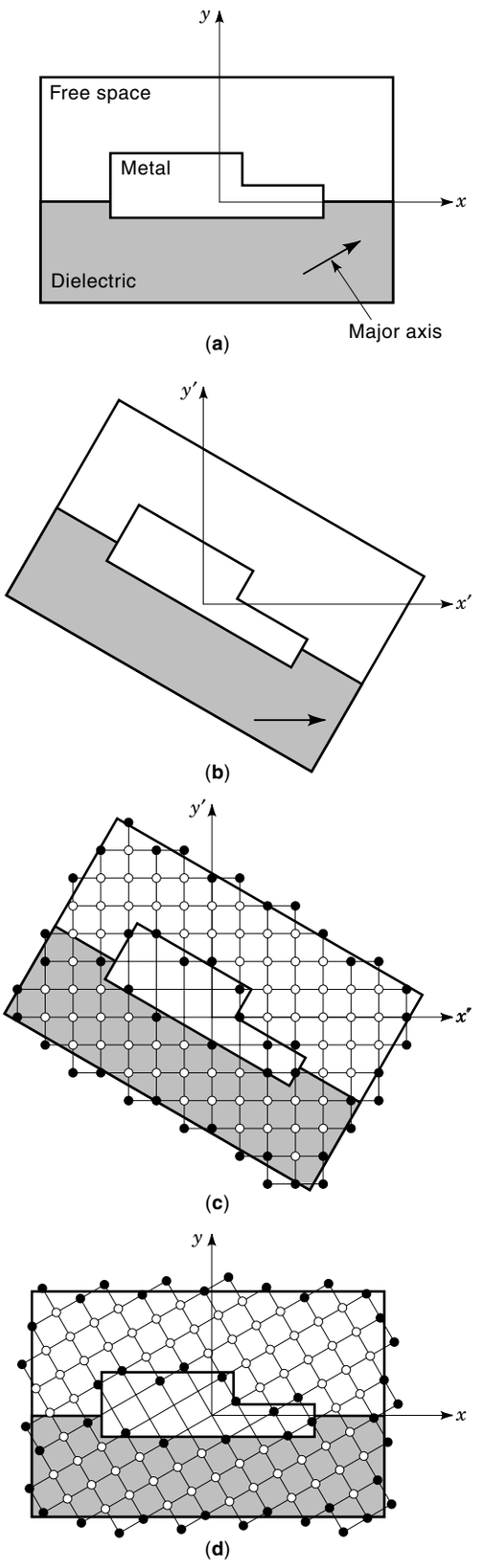

Figure 12. Graphical representation of coordinate transformation for inhomogeneous anisotropic dielectric with diagonal permittivity tensor.

However, the computational overhead associated with the pre- and postprocessing can be significant, since the geometry is usually complicated by such transformations.

SAMPLE NUMERICAL RESULTS

To illustrate the versatility of FDM in solving engineering problems that involve arbitrary geometries and inhomogeneous materials, consider the cross section of a microwave field effect transistor (FET) shown in Fig. 13. Note that this device is composed of many different materials, each of different thickness and cross-sectional profile. The FET is drawn to scale, with the 1 μm thickness of the buffer layer serving as a reference. FDM can be used to calculate the potential and field distribution throughout the entire cross section of the FET. This information can be used by the designer to investigate such effect as material breakdown near the metallic electrodes. In addition, the computed field information can be used to determine the parasitic capacitance matrix of the structure, which can be used to improve the circuit model of this device and is very important in digital circuit design. Finally, it should be noted that the losses associated with the silicon can also be computed using FDM as shown in Eq. (25).

It should be added that in addition to displaying the potential distribution over the cross section of the FET, Fig. 13 also illustrates the implementation of open boundary truncation operators. Since the device is located in an open boundary environment, it was necessary to artificially truncate the computation space (or 2-D grid). Note that, as demonstrated in Ref. 25, only the first-order operator was sufficient to obtain accurate representation of the potential in the vicinity of the electrodes as well as near the boundary truncation surface.

A sample with three-dimensional geometry that can be easily analyzed with the FDM is shown in Fig. 14. The insulator in the multilayer ceramic capacitor is assumed to be anisotropic barium titanate dielectric, which is commonly used in such components. The permittivity tensor is diagonal and its elements are $\epsilon_{xx} = 1540$, $\epsilon_{yy} = 290$, and $\epsilon_{zz} = 1640$. To demonstrate the effect of anisotropy on this passive electrical component, its capacitance was calculated as a function of the misalignment angle between the crystal axes of the insulator and the geometry of the structure (see Fig. 15).

For the misalignment angle (or rotation of axes) in the yz plane, the capacitance of this structure was computed. The results of the computations are plotted in Fig. 16. Note that the capacitance varies considerably with the rotation angle. Such information is invaluable to a designer, since the goal of the design is to maximize the capacitance for the given dimensions of the structure.

The above examples are intended to demonstrate the applicability of FDM to the solution of practical engineering boundary-value problems. FDM has been used extensively in analysis of other practical problems. The interested reader can find additional examples where FDM was used in Refs. 31–37.

SUMMARY

Since the strengths and weaknesses of FDM were mentioned throughout this article, as were the details dealing with the derivation and numerical implementation of this method,

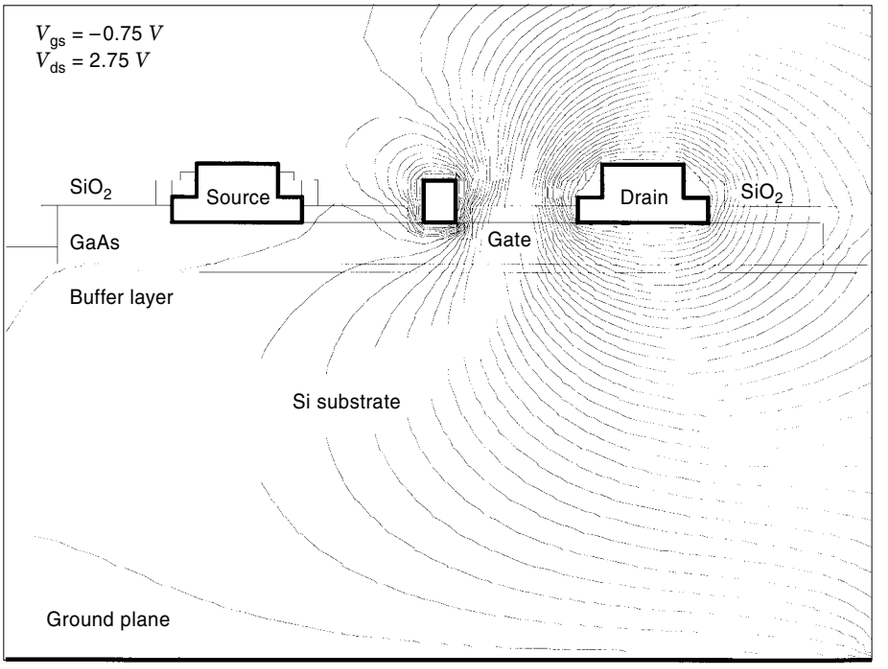

Figure 13. Equipotential map of dc-biased microwave FET. From Computer-aided quasi-static analysis of coplanar transmission lines for microwave integrated circuits using the finite difference method, B. Beker and G. Cokkinides, *Int. J. MIMICAE,* **4** (1): 111–119. Copyright © 1994, Wiley.)

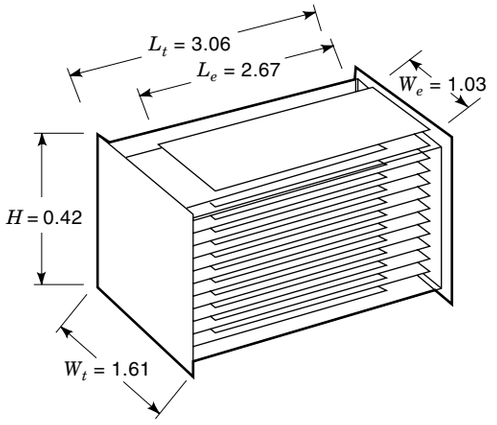

Figure 14. Geometry of a multilayer ceramic chip capacitor. All dimensions are in millimeters.

they need not be repeated. However, the reader should realize that FDM is best suited for boundary-value problems with complex geometries and arbitrary material composition. The complexity of the problem is the primary motivating factor for investing the effort into developing a general-purpose volumetric analysis tool.

ACKNOWLEDGMENTS

The authors wish to express their sincere thanks to many members of the technical staff at AVX Corporation for initiating, supporting, and critiquing the development and implementation of many concepts presented in this article, as well as for suggesting practical uses of FDM. Many thanks also go to Dr. Deepak Jatkar for his help in extending FDM to general anisotropic materials.

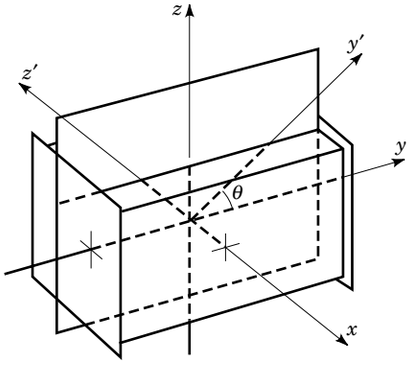

Figure 15. Definition of rotation angle for anisotropic insulator.

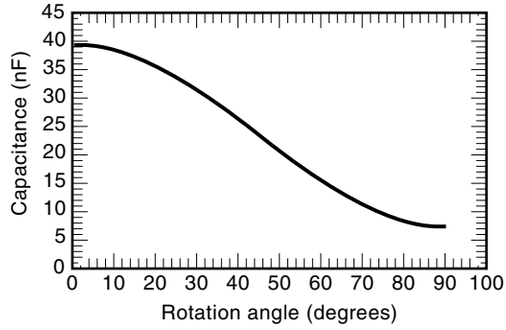

Figure 16. Capacitance of multilayer chip capacitor as a function of rotation angle of the insulator.

BIBLIOGRAPHY

1. H. Liebmann, *Sitzungsber. Bayer. Akad. München,* 385, 1918.
2. R. V. Southwell, *Relaxation Methods in Engineering Science,* Oxford: Clarendon Press, 1940.
3. R. V. Southwell, *Relaxation Methods in Theoretical Physics,* Oxford: Clarendon Press, 1946.
4. H. E. Green, The numerical solution of some important transmission line problems, *IEEE Trans. Microw. Theory Tech.,* **17** (9): 676–692, 1969.
5. F. Sandy and J. Sage, Use of finite difference approximation to partial differential equations for problems having boundaries at infinity, *IEEE Trans. Microw. Theory Tech.,* **19** (5): 484–486, 1975.
6. G. Liebmann, Solution to partial differential equations with resistance network analogue, *Br. J. Appl. Phys.,* **1** (4): 92–103, 1950.
7. K. S. Yee, Numerical solution of initial boundary value problems involving Maxwell's equations in isotropic media, *IEEE Trans. Antennas Propag.,* **14** (3): 302–307, 1966.
8. A. Taflove, *Computational Electrodynamics: The Finite-Difference Time-Domain Method,* Boston, MA: Artech House, 1995.
9. N. N. Rao, *Elements of Engineering Electromagnetics,* 4th ed., Englewood Cliffs, NJ: Prentice-Hall, 1994.
10. S. R. H. Hoole and P. R. P. Hoole, *A Modern Short Course in Engineering Electromagnetics,* New York: Oxford University Press, 1996.
11. T. G. Jurgens, A. Taflove, K. Umashankar, and T. G. Moore, Finite-difference time-domain modeling of curved surfaces. *IEEE Trans. Antennas Propag.,* **40** (4): 357–366, 1992.
12. M. Naghed and I. Wolf, Equivalent capacitances of coplanar waveguide discontinuities and interdigitated capacitors using three-dimensional finite difference method, *IEEE Trans. Microw. Theory Tech.,* **38** (12): 1808–1815, 1990.
13. M. F. Iskander, *Electromagnetic Fields & Waves,* Englewood Cliffs, NJ: Prentice-Hall, 1992, Section 4.8.
14. R. Haberman, *Elementary Applied Partial Differential Equations with Fourier Series and Boundary Value Problems,* Englewood Cliffs, NJ: Prentice-Hall, 1983, Chapter 13.
15. L. Lapidus and G. H. Pinder, *Numerical Solutions of Partial Differential Equations in Science and Engineering,* New York: Wiley, 1982.
16. W. F. Tinney and J. W. Walker, Direct solution of sparse network equations by optimally ordered triangular factorization, *IEEE Proc.,* **55** (11), 1967.
17. W. T. Press, B. P. Flanney, S. A. Teukolsky, and W. T. Vetterling, *Numerical Recipes: The Art of Scientific Computing,* 2nd ed., Cambridge: Cambridge University Press, 1992, Section 2.7.
18. Y. Saad, *Iterative Methods for Sparse Linear Systems,* Boston: PWS Publishing Co., 1996.
19. G. H. Golub and C. F. Van Loan, *Matrix Computations,* 3rd ed., Baltimore: Johns Hopkins University Press, 1996, Chapter 10.
20. R. E. Philips and F. W. Schmidt, Multigrid techniques for the numerical solution of the diffusion equation, *Num. Heat Transfer,* **7**: 251–268, 1984.
21. J. H. Smith, K. M. Steer, T. F. Miller, and S. J. Fonash, Numerical modeling of two-dimensional device structures using Brandt's multilevel acceleration scheme: Application to Poisson's equation, *IEEE Trans. Comput.-Aided Des. Integr. Circuit Syst.,* **10** (6): 822–824, 1991.
22. A. Kherib, A. B. Kouki, and R. Mittra, Higher order asymptotic absorbing boundary conditions for the finite element modeling of two-dimensional transmission line structures, *IEEE Trans. Microw. Theory Tech.,* **38** (10): 1433–1438, 1990.
23. A. Kherib, A. B. Kouki, and R. Mittra, Asymptotic absorbing boundary conditions for the finite element analysis of three-dimensional transmission line discontinuities, *IEEE Trans. Microw. Theory Tech.,* **38** (10): 1427–1432, 1990.
24. R. K. Gordon and H. Fook, A finite difference approach that employs an asymptotic boundary condition on a rectangular outer boundary for modeling two-dimensional transmission line structures. *IEEE Trans. Microw. Theory Tech.,* **41** (8): 1280–1286, 1993.
25. B. Beker and G. Cokkinides, Computer-aided analysis of coplanar transmission lines for monolithic integrated circuits using the finite difference method, *Int. J. MIMICAE,* **4** (1): 111–119, 1994.
26. T. L. Simpson, Open-boundary relaxation, *Microw. Opt. Technol. Lett.,* **5** (12): 627–633, 1992.
27. D. Jatkar, *Numerical Analysis of Second Order Effects in SAW Filters,* Ph.D. Dissertation, University of South Carolina, Columbia, SC, 1996, Chapter 3.
28. S. R. Hoole, *Computer-Aided Analysis and Design of Electromagnetic Devices,* New York: Elsevier, 1989.
29. V. K. Tripathi and R. J. Bucolo, A simple network analog approach for the quasi-static characteristics of general, lossy, anisotropic, layered structures, *IEEE Trans. Microw. Theory Tech.,* **33** (12): 1458–1464, 1985.
30. R. E. Collin, *Foundations for Microwave Engineering,* 2nd ed., New York: McGraw-Hill, 1992, Appendix III.
31. B. Beker, G. Cokkinides, and A. Templeton, Analysis of microwave capacitors and IC packages, *IEEE Trans. Microw. Theory Tech.,* **42** (9): 1759–1764, 1994.
32. D. Jatkar and B. Beker, FDM analysis of multilayer-multiconductor structures with applications to PCBs, *IEEE Trans. Comp. Pack. Manuf. Technol.,* **18** (3): 532–536, 1995.
33. D. Jatkar and B. Beker, Effects of package parasitics on the performance of SAW filters, *IEEE Trans. Ultrason. Ferroelect. Freq. Control,* **43** (6): 1187–1194, 1996.
34. G. Cokkinides, B. Beker, and A. Templeton, Direct computation of capacitance in integrated passive components containing floating conductors, *IEEE Trans. Comp. Pack. Manuf. Technol.,* **20** (2): 123–128, 1997.
35. B. Beker, G. Cokkinides, and A. Agrawal, Electrical modeling of CBGA packages, *Proc. IEEE Electron. Comp. Technol. Conf.,* 251–254, 1995.
36. G. Cokkinides, B. Beker, and A. Templeton, Cross-talk analysis using the floating conductor model, *Proc. ISHM-96, Int. Microelectron. Soc. Symp.,* 511–516, 1996.
37. B. Beker and T. Hirsch, Numerical and experimental modeling of high speed cables and interconnects, *Proc. IEEE Electron. Comp. Technol. Conf.,* 898–904, 1997.

BENJAMIN BEKER
GEORGE COKKINIDES
MYUNG JIN KONG
University of South Carolina